Dynamic Model of the Weighing Process of an Industrial Combination Scale: Model Development and Simulative Analysis of the Product Impact Force

Felix Profe[1][a], Lucas Kostetzer[2][b] and Christoph Ament[1][c]

[1]Chair of Control Engineering, University of Augsburg, 86159 Augsburg, Germany
[2]CADFEM Germany GmbH, 85567 Grafing bei München, Germany

Abstract: This work shows a weighing product model that characterizes the processes of product impact during the weighing procedure of a combination scale. Unfortunately, the product impact force does not exist as a sensor quantity and is difficult to measure. Another complicating factor in developing a product model is the large variety of products and their fall behaviour. Even with identical product properties, falling comprises strong stochastic influence. With the help of a discrete element method simulation model it was possible to directly calculate the product impact force. More than 20 different products were tested. The simulation can reproduce the random fall behaviour. Based on these analyses, a real-time capable product model was derived. The model is able to generate impact curves based on portion weight, particle weight, impact time, drop height, and impact duration. Impact duration and time of impact of an individual particle are changing based on random variables. Due to simplifications, restitution coefficient and particle shape is not considered. With larger particles there are deviations in comparison of simulation and product model. Due to the low computational effort, the model could be used, for example, as a system input for a real-time capable model of a weighing station.

1 INTRODUCTION

This work shows a weighing product model that could represent the processes of product impact during the weighing procedure of a combination scale (CS). Due to the low computational effort, the model could be used, for example, as a system input for a real-time capable model of a weighing station.

1.1 Combination Scale

Figure depicts a CS. According to Oehring and Thiele (1989) CS are particularly suitable for frozen products, in the confectionery industry and for salad products. For these products, a desired final weight (target weight) can be achieved more precisely (and without large overestimation) by suitably combining pre-portioned partial quantities. In principle, all common weighing products can be filled with CS, but there is no major advantage with free-flowing and granular products. CS have a larger number of individual weighing stations from which a computer determines the optimum combination for the specified nominal filling weight. Figure 1 shows the CS components attached to a frame. A distribution cone is located at the top centre.
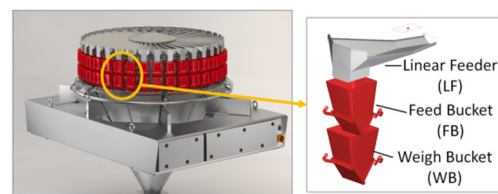

Figure 1: Combination scale (left) and section of a weighing station with linear feeder, feed bucket and weigh bucket (right) according to Profe and Ament (2022).

[a] https://orcid.org/0009-0005-7026-9018
[b] https://orcid.org/0000-0003-3820-233X
[c] https://orcid.org/0000-0002-6396-4355

Around the distribution cone, linear feeders (LF) are arranged in a circle towards the outside. Feed buckets (FB) are located below the LF, followed below by weighing buckets (WB), both buckets in red. Finally, chutes and a funnel are attached below.

The piece goods are fed from above and supplied to the WB via distribution cone, LF, and FB. The weight of the partial quantity is determined when the product is in the WB. Each WB is connected to a load cell (Profe and Ament, 2022).

1.2 Challenges and Application of Product Model

A detailed model description of the weighing process is of high relevance for the development and improvement of weighing systems. A model can be used for example for digital twins, virtual experiments to understand the cause-effect relationship, control systems (e.g. as an observer), and, in general, to generate virtual data (Profe and Ament, 2022). Figure 1 shows the block diagram of the system *weighing station*. The output is the weighing signal from the associated load cell. The system *weighing station* includes WB, which is connected to a load cell. The system input corresponds to the product impact force (PIF).

The PIF is the force created by the partial quantity falling out of the FB and hitting the WB (weighing station). A detailed knowledge of the PIF is important for fast and accurate weighing.
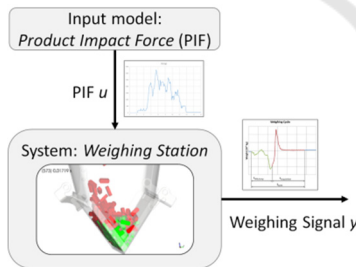

Figure 2: System *Weighing station* with product impact force as input and weighing signal as output.

For this purpose, a model approach for a so-called *Product Model* will be presented in this paper. Models of weighing stations were presented in the publications of Eckstein and Ament (2019) and Profe and Ament (2022). However, these models work without a product model although this could increase the weight acquisition speed or the accuracy of results. Wente (1992) and Gilman and Bailey (2005) presented force curve models of weighing stations, but in these models, there is no specific link

to the weighing goods of a CS. A product model has not yet been used because the impact force does not exist as a sensor quantity. PIF is even difficult to measure directly. Only the system response (weighing signal) is available. Another complicating factor in developing a product model is the large variety of products to be weighed and the varying fall behaviour of the product. Even with identical product properties, falling comprises strong stochastic influence. In this work the PIF is determined with the help of the *Discrete Element Method (DEM)*.

2 DEM SIMULATION MODEL

A direct measurement of the PIF was not carried out on a real test setup, due to the challenges to generate controlled and reproducible data. Instead, a virtual model was created (see Figure 2). The model consists of LF, FB and WB. It is a section of a CS. There is product in LF, FB and WB. In contrast to the real scale, the product falls directly into LF (see product input in Figure 2) instead of the distribution cone. The flaps of FB and WB are able to open and close the respective buckets.
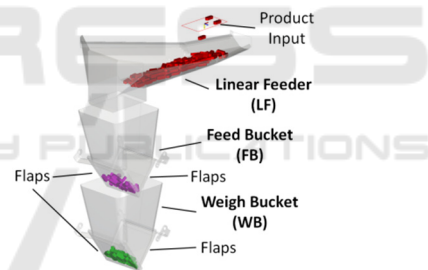

Figure 3: Virtual simulation model of a weighing station.

Table 1: Timing of LF, FB and WB within a weighing cycle.

LF					Vibrating
FB			Opening	Closing	
WB	Opening	Closing			
			Time →		

Table 1 depicts the sequence of the processes running in parallel in the virtual model. The processes start in the third row with opening and closing of WB. Shortly after the WB flaps are closed again, new product falls into WB. Parallel to WB, FB opens with a time delay. The flaps of FB start to open at the moment when WB flaps are fully open. After the FB flaps are closed, new product can be added. Therefore LF starts to vibrate. FB is filled

again. The whole process is then repeated and starts with WB opening again.

2.1 Result Evaluation Methods

The PIF is analysed in the vertical direction. The left side of Figure 3 shows the mesh of the WB flaps on which the impact force evaluation is performed. Parallel to the evaluation of the force, the total particle mass in the WB is determined over time. For this purpose, an evaluation block is placed over WB (see right side of Figure 3). Particles with a velocity of less than 0.1 m/s belongs to the WB mass. This allows an objective assessment of how long the particles take to settle down (analysis of fall behaviour).
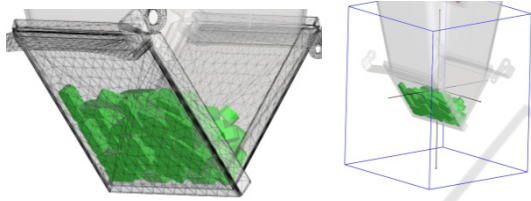

Figure 4: Mesh of the WB flaps for evaluation of force (left). Borders of cubic WB evaluation block in blue (right).

2.2 Mathematical Models

The simulations in this work were performed using DEM. According to Ansys Inc. (2023) DEM is a numerical technique for predicting the behaviour of bulk solids. The equations of motion for every individual particle are numerically integrated over time. For this process the total force on a particle needs to be known. The total force is the resultant of contact forces (between particles and with boundary) and body forces (e.g. gravity). When considering the PIF, the contact force models play an important role. According to Walton and Braun (1986) *Hysteric Linear Spring* was used as normal force model. It does not use viscous damping terms. Energy is dissipated only upon contact with the boundary or other particles. The contact force law is defined as follows (Walton and Braun, 1986):

$$F_n^t = \begin{cases} \min(A, B) & if\ \Delta s_n \geq 0 \\ \max(B, \lambda \cdot A) & if\ \Delta s_n < 0 \end{cases} \quad (1)$$

$$A = K_{nl} \cdot s_n^t \quad (2)$$

$$B = F_n^{t-\Delta t} + K_{nu} \cdot \Delta s_n \quad (3)$$

$$\Delta s_n = s_n^t - s_n^{t-\Delta t} \quad (4)$$

F_n^t and $F_n^{t-\Delta t}$ are the normal elastic-plastic contact forces at the current time t and at the previous time $t - \Delta t$. Δt is the timestep size. s_n^t and $s_n^{t-\Delta t}$ are the normal overlap values at the current time t and the previous time $t - \Delta t$. Δs_n is the incremental contact normal overlap at time t. A positive value means an approach and a negative value a separation. The index n stands for normal force. λ is a dimensionless small constant with the value 0.001 (Ansys Inc., 2023).

The equivalent stiffness K_{nl} for loading and K_{nu} for unloading are formed as follows:

$$\frac{1}{K_{nl}} = \begin{cases} \dfrac{1}{K_{nl,p1}} + \dfrac{1}{K_{nl,p2}} \\ \dfrac{1}{K_{nl,p}} + \dfrac{1}{K_{nl,b}} \end{cases} \quad (5)$$

$$K_{nu} = \frac{K_{nl}}{\varepsilon^2} \quad (6)$$

ε is the coefficient of restitution. $K_{nl,p1}$ is the contact stiffness of particle 1 and $K_{nl,p2}$ is the contact stiffness of particle 2 in case there is an interaction between two particles. $K_{nl,p}$ is the contact stiffness of a particle in general and $K_{nl,b}$ is the contact stiffness of the boundary. Figure 4 shows the underlying series connection between particle and boundary with $K_{nl,p}$ and $K_{nl,b}$ defined in (5). $K_{nl,p}$ and $K_{nl,b}$ are calculated of the Young's modulus E_p or E_b and the particle size L:

$$K_{nl,p} = E_p \cdot L \quad (7)$$

$$K_{nl,b} = E_b \cdot L \quad (8)$$
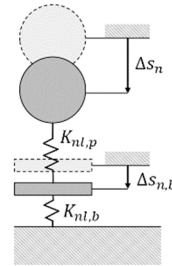

Figure 5: Series connection of contact stiffnesses between particle and boundary.

The following values were used in the simulations: WB as boundary has a E_b of 100 000 MPa. The particles have a E_p of 100 MPa. Due to the series connection (Figure 4 and (5)), we see that E_b has almost no influence, since it is many times greater than E_p. It follows that in this case the

stiffness of the particle, $K_{nl,p}$ has a large influence on the impact force and the stiffness of WB $K_{nl,b}$ a small one assuming $K_{nl,b}$ is much stiffer than $K_{nl,p}$.

The following modules of the simulation software *Ansys Rocky 2023 R1* were used for evaluation: *Boudary Collision Statistics*, *Contacts Overlap Monitor*, and *SPH Density Monitor*.

3 REAL-TIME CAPABLE PRODUCT MODEL

With the help of the DEM simulation model presented in the previous section, reality was approximated in order to analyse the fall behaviour and the impact curves. The virtual model serves as a substitute for real experiments due to the effort required for experiments. However, the DEM simulation model is very complex and not real-time capable due to the higher computational effort. Therefore, a simpler approach is now presented: The so-called *Product Model*. It is a model with lower complexity. This means that some assumptions have to be made. First, air resistance is not considered (neither in DEM simulation nor in *Product Model*). Second, the impact has no rebound ($\varepsilon = 0$). Third, the *Product Model* uses point masses. Fourth, the impact surface is plane and horizontal (no slanted flaps). Fifth, E_p or E_b is not relevant. Sixth, there is no interaction between particles. Seventh, each particle generates a rectangular pulse on impact according to Wente (1992).
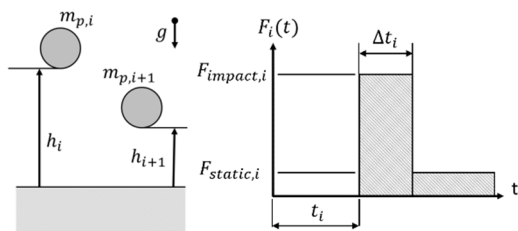
3.1 Mathematical Model

Figure 6: Free falling of two masspoints due to gravity (left). Force curve of rectangular impact pulse and static weight force (right).

Figure 5 (left) shows two mass points. $m_{p,i}$ is the mass of the *i*-th point or particle. $m_{p,i+1}$ is the mass of the *i+1*-th mass point. In total there are *n* different mass points. The two mass points shown are dropped from heights h_i and h_{i+1} from rest (initial

velocity = 0). Just before impact, the *i*-th mass point has the impact velocity (Stronge, 2018):

$$v_i = \sqrt{2 \cdot g \cdot h_i} \qquad (9)$$

g is the acceleration due to gravity at 9.81 m/s. By integration of Newton's axiom the pulse *I* is obtained (Stronge, 2018) by:

$$I = \int_0^t F_i(t) \cdot dt = m_{p,i} \cdot v_{2,i} - m_{p,i} \cdot v_{1,i} \qquad (10)$$

$F_i(t)$ is the contact force of particle *i*. Index *1* means immediately before impact and index *2* means after impact. Due to the assumption $\varepsilon = 0$, the particle is completely decelerated ($v_{2,i} = 0$). Thus, for each individual particle, the impact pulse can be set up as follows:

$$I_i = m_{p,i} \cdot v_i \qquad (11)$$

For simplicity, the integral of the impact force of a single particle is modelled as a rectangle with

$$I_i = F_{impact,i} \cdot \Delta t_i \qquad (12)$$

where Δt_i is the duration of a single particle impact. Thus the impact force is:

$$F_{impact,i} = \frac{I_i}{\Delta t_i} \qquad (13)$$

The moment of impact of an individual particle results from the fall time:

$$t_i = \sqrt{\frac{2 \cdot h_i}{g}} \qquad (14)$$

Figure 5 (right) shows the rectangular force curve over the course of time. After the impact has occurred, the force $F_i(t)$ switches to the static weight fraction $F_{static,i}$.

The curve of the total impact force is given by the sum of all particle forces according to Wente (1992):

$$F(t_i) = \sum_{i=1}^n F_i(t_i) \qquad (15)$$

3.2 Model Parameters

Figure 6 shows the inputs and outputs of the *Product Model*. Using the target weight m_{target} and the piece weight m_p, the number of particles is calculated with

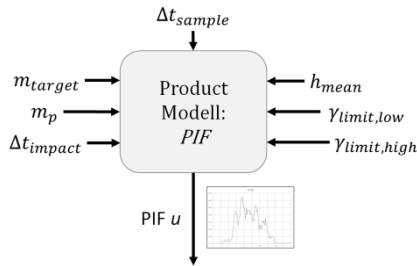$$n = \frac{m_{target}}{m_p} \qquad (16)$$

Figure 7: input and output parameters of the *Product Model*.

The number of pieces is rounded if the target weight is not a multiple of the piece weight. Δt_{impact} specifies the duration of the single pulse. With this approach, all single pulses are equal. Thus applies:

$$\Delta t_i = \Delta t_{impact} \tag{17}$$

Δt_{sample} is the time step size and h_{mean} is the mean drop height of the particles.

In order to represent the randomly occurring fall behaviour, the drop height of the individual particle is modelled as a normal distributed random variable:

$$h_i \sim \mathcal{N}(h_{mean}, \sigma_{height}) \tag{18}$$

h_i determines the fall time t_i of the individual particle. The difference between the shortest and longest fall time (total time duration) is set by the standard deviation σ_{height}. It is assumed that the majority of impact curves have the same total duration. However, there are differing impact situations. Therefore σ_{height} is also a random variable. It applies:

$$\sigma_{height} \sim \mathcal{N}(\mu_{duration}, \sigma_{duration}) \tag{19}$$

$$\mu_{duration} = \gamma_{limit,low} \tag{20}$$

$$\sigma_{duration} = \frac{\gamma_{limit,high} - \gamma_{limit,low}}{3} \tag{21}$$

$\gamma_{limit,low}$ is the lower limit of σ_{height} and $\gamma_{limit,high}$ is the upper limit. σ_{height} is cut off for smaller values than $\gamma_{limit,low}$:

$$\sigma_{height} = \gamma_{limit,low} \quad if \quad \sigma_{height} < \gamma_{limit,low} \tag{22}$$

4 PRODUCT EXPERIMENTS

Experiments were conducted with both models – DEM simulation model and *Product Model*. The sweet marshmallow like product in Figure 7 on the left side is the original product. It looks like Santa Claus. From now on the product will be called

Marshmallow (MM) or just product in this paper. The product has dimensions of 55 mm × 23 mm × 16 mm and an average piece weight of 5.832g. The density is 300 kg/m³.
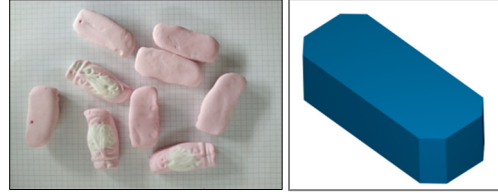

Figure 8: Original sweet marshmallow (MM) like product (left) and simplified particle model (right).

Table 2: Piece weight m_p and piece number n depending on *SF*.

SF	Piece Number n	Piece Weight m_p
0.1	1000	0.1%
0.3	37	2.7%
0.4	16	6.4%
0.7	3	34.3%
1.0	1	100.0%

In the simulation, a simplified representation is chosen (Right side of Figure 7). The product is a cuboid with a chamfer at each of the four corners. In the *Product Model*, only the piece weight of the product is of interest, since the masses are point masses. In the following investigations, the size and thus also the piece weight is changed with a scaling factor (SF). For this purpose, the length l, width w, and depth d of the original MM product are changed respectively. Thus the scaled volume $V_{Scaling}$ is defined:

$$V_{Scaling} = SF^3 \cdot l \cdot w \cdot d \tag{23}$$

Table 2 shows the piece weight m_p and piece number n as a function of *SF* for selected sizes.

4.1 Overview of Studies

Virtual experiments are carried out with the aid of the DEM simulation model. The *Product Model* was derived on the basis of these findings.

First, a comparison of PIF is made between DEM simulation and *Product Model* at a target weight of 50g (*SF=1* and *SF=0.3*). Subsequently, the target weight is increased to 100g at *SF=0.4*. There the duration of PIF is compared. Then ε is increased from $\varepsilon=0.1$ to $\varepsilon = 0.7$. Finally, the maximum PIF is examined as a function of *SF*.

In the case of the *Product Model*, the tests on ε cannot be carried out, since the model does not include this property.

4.2 DEM Simulation Setup

The model-specific parameters of the simulations are given below. If not explicitly mentioned, these settings are used for all simulations. Static friction μ_{static} and dynamic friction $\mu_{dynamic}$ have the same value in this work ($\mu_{static} = \mu_{dynamic} = \mu$). $\mu = 0.7$ is used between particles. From particle to boundary (in our case, among others, the WB flaps) $\mu = 0.3$. Both are default settings. If not otherwise mentioned, $\varepsilon = 0.1$.
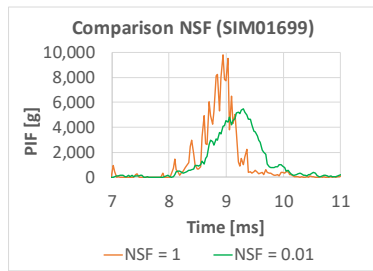

Figure 9: Comparison of the impact curve depending on *NSF*.

To save calculation time, a Numerical Softening Factor (*NSF*) of 0.01 was used instead of the default value *NSF=1*. All stiffness parameters (e.g. in (1) - (3)) are multiplied by *NSF* (Lommen, Schott and Lodewijks, 2014). This can result in overlapping bodies, which in our case has a large effect on the impact force (see Figure 8). A lower *NSF* is more suitable for the presented application due to the load cell and its elastic spring effect. Global deformations prolong the contact period, reduce the maximum contact force and transfer significant energy into structural vibrations according to Stronge (2018).
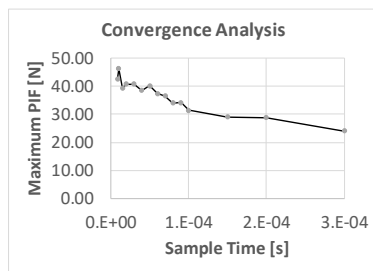

Figure 10: Convergence analysis of the maximum force of the impact curve depending of sample time.

The stiffness is used to determine the time step size of the calculation. For *NSF=1* the time step size is 5.87e-7s and for *NSF=0.01* the time step size is 5.87e-6s. In addition, the output time step size (sample time) has to be defined separately. Figure 9 shows a convergence analysis of the sample time. It

has no influence on the calculation accuracy, but on the output accuracy. For reasons of calculation time, memory requirements and accuracy, 30μs was chosen as sample time.

4.3 Product Model Setup

For the *Product Model* $\Delta t_{impact} = 500\mu s$ is chosen. The value was fitted from the impact duration of a single particle in DEM simulation results.

5 RESULTS

In the following, the PIF is converted into a weight value with:

$$PIF(t_i) = \frac{F(t_i)}{g} \qquad (24)$$

This allows a better view of the ratio of the maximum value of PIF to the static weight.

5.1 Comparison SF=1

Figure 10 shows the first comparison between simulation and *Product Model* (50g MM, *SF*=1). 7 pieces fall onto WB flaps. *Product Model* generates exactly 7 small impacts. In the simulation model there are more than 7 impacts. The maximum force is between 4kg and 5kg.
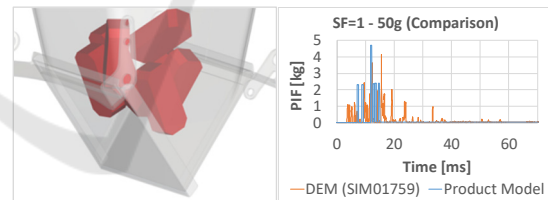

Figure 11: Falling of 50 g MM with *SF=1*. Comparison of simulation and *Product Model* with a root mean square error (*RMSE*) of 464.098g.
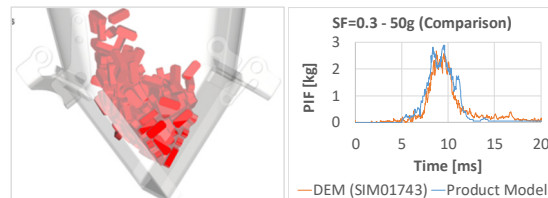
5.2 Comparison SF=0.3

Figure 12: 50g MM with *SF=0.3*. Comparison of *Product Model* and simulation with *RMSE = 94.301g*.

Figure 11 shows a comparison between simulation and *Product Model* with *SF=0.3*. The maximum force is between 2kg and 3kg. The duration of the highest peak is about 10ms.

5.3 Duration of Impact at 100g

The static weight is increased to 100g with *SF=0.4*. Figure 12 depicts a comparison of DEM simulation and *Product Model*. The simulation shows a duration of about 40 to 50ms. There are two peaks. The first peak is higher than the second. The duration of PIF at *Product model* is about 50ms. There is only one higher peak at about 30ms.
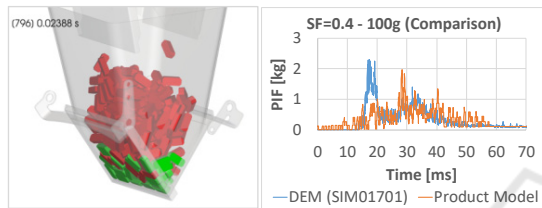

Figure 13: 100g MM with *SF=0.4* after 23.88ms (left). Comparison of simulation and *Product Model* (right).

5.4 Variation of Restitution Coefficient

PIF in Figure 13 (right) with $\varepsilon = 0.7$ is very similar to PIF with $\varepsilon = 0.1$ (left side of Figure 13). ε has an influence on K_{nu} but not on K_{nl} according to (5) and (6). Nevertheless, the rebounding particles change the PIF of the following particles. Table 3 shows the deviation of the PIF when changing ε from $\varepsilon = 0.1$ to a higher value. In addition, with a higher ε the particles are longer in motion (comparison of static weight in Figure 13 left to right). With $\varepsilon = 0.7$ the static weight shows the first particle in rest at about 45ms (see right side of Figure 13). With $\varepsilon = 0.1$ this occurs at about 25ms (Figure 13 left).
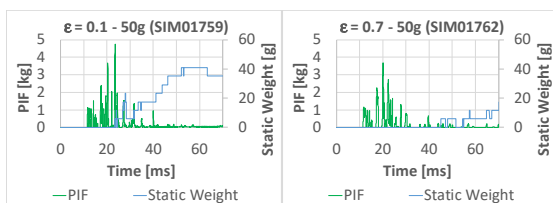

Figure 14: PIF and static weight of 50g *SF=1* and $\varepsilon = 0.1$ (left) and $\varepsilon = 0.7$ (right). Due to the rebound, many particles are still in motion after 70ms with $\varepsilon = 0.7$ (blue).

Table 3: RMSE of PIF to $\varepsilon = 0.1$.

ε	RMSE [g]
0.3	226.419
0.5	267.293
0.7	275.186

5.5 Fluctuation and Variation of SF

Figure 14 shows the ratio of maximum PIF to static weight as a function of *SF*. There are large fluctuations, which is caused by the random fall behaviour. The trend is that PIF gets higher *SF* increases.
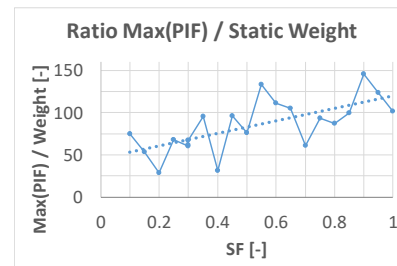

Figure 15: Ratio of maximum force to static weight as a function of *SF*.

6 DISCUSSION

Using the DEM simulation model, it was possible to directly calculate the PIF, which is difficult to measure with a sensor in an experiment. A large number of test series with more than 20 different products could be carried out in the simulations. Likewise, the random fall behaviour during impact could be simulated. Based on these analyses, a real-time capable product model was derived. The model could generate impact curves based on target weight, piece weight, impact time, mean drop height, and impact duration. Total impact duration and time of impact of an individual particle are changing based on random variables. Due to simplifications, restitution coefficient and shape of the particle are not considered. This means that only one impact per particle is mapped at a PIF curve. For larger particles, as in the case of the original size of the test product MM, there are therefore deviations in comparison of DEM simulation and *Product Model* (see Figure 10). If the buckets are filled to a greater extent, delayed double peaks occur (see DEM in Figure 12). The Product is hindered in the FB when falling (behaviour like in an hourglass). This is also not represented by the *Product Model*. However, if the bucket size is selected correctly, this situation should not occur in practice.

In summary this study shows a weighing product model that could represent the process of product impact during the weighing procedure of CS. This paper analysed the PIF isolated from the system. However, the PIF is dependent on the stiffness of the system *weighing station* (see (5) and Figure 4). Therefore, the weighing station and its effect on the PIF should be taken into account in future studies. So far, a comparison has been made from the *Product Model* to a virtual test (DEM simulation). However, it would be very desirable if in future work a comparison could be made with measurements on a real weighing station and exam-ples from literature (with the extended model). Stronge (2018) shows approaches for impact against flexible structures.

REFERENCES

Ansys Inc. (2023) 'Rocky DEM Technical Manual: Version 2023 R1'.

Eckstein, S. and Ament, C. (2019) 'Modellbasierte Signalschätzung eines industriellen Sensorsystems', in Meurer, T. and Woittennek, F. (eds.) *Tagungsband.* Kiel: Kiel University, pp. 368–369.

Gilman, A. and Bailey, D. (2005) 'High-speed Weighing Using Impact on Load Cells', *TENCON 2005 - 2005 IEEE Region 10 Conference, TENCON 2005 - 2005 IEEE Region 10 Conference*, Melbourne, Australia, 2005: IEEE, pp. 1–6. doi: 10.1109/TENCON.2005.301118

Lommen, S., Schott, D. and Lodewijks, G. (2014) 'DEM speedup: Stiffness effects on behavior of bulk material', *Particuology*, 12, pp. 107–112. doi: 10.1016/j.partic.2013.03.006

Oehring, H.-A. and Thiele, J. (1989) 'Selbsttätige Waagen zum diskontinuierlichen Wägen und Abwägen', in Kochsiek, M. (ed.) *Handbuch des Wägens,* 2nd edn. Wiesbaden: Vieweg+Teubner Verlag; Imprint, pp. 423–426.

Profe, F. and Ament, C. (2022) 'ODE System Identification of a Dynamic Weight Acquisition Process Using Feedforward Neural Networks', *IFAC-PapersOnLine*, 55(20), pp. 31–36. doi: 10.1016/j.ifacol.2022.09.068

Stronge, W.J. (2018) *Impact mechanics*. 2nd edn. Cambridge: Cambridge University Press. Available at: https://www.cambridge.org/core/books/impact-mechanics/DE106F5C9A5DF715940D9948F138B972.

Walton, O.R. and Braun, R.L. (1986) ' Viscosity, granular‑temperature, and stress calculations for shearing assemblies of inelastic, frictional disks', *Journal of Rheology*, 30(5), pp. 949–980. doi: 10.1122/1.549893

Wente, H. (1992) *Ein Beitrag zur intelligenten Dämpfung schwingungsfähiger elastischer Systeme unter besonderer* Berücksichtigung *elektromechanischer Waagen*. (Verein Deutscher Ingenieure, 171). Düsseldorf: VDI Verl.